Energy Materials

Supplementary Materials

Electronically active Sn nanosheets enable Sn-to-Pt interfacial charge redistribution for acidic and alkaline hydrogen evolution

Yifan Huang[1,#], Hailin Jiao[2,#], Bowen Bai[1,*], Lin Zhao[1], Li Liu[3,4], Tao Yu[1], Futang Li[1], Min Zhao[2], Jingkun Wang[2], Quan Bai[1], Jin Li[1,*], Xuesong Leng[1,*]

[1]Research Institute of Physical Sciences in Special Environments, Harbin Institute of wjTechnology (Shenzhen), Shenzhen 518055, Guangdong, China.
[2]College of Physics and Optoelectronics, Shanxi Key Lab of Photovoltaic Technology and Application, Key Lab of Advanced Transducers and Intelligent Control System, Ministry of Education, Taiyuan University of Technology, Taiyuan 030024, Shanxi, China.
[3]School of Materials Science and Engineering, Harbin Institute of Technology (Shenzhen), Shenzhen 518055, Guangdong, China.
[4]National Key Laboratory of Precision Hot Processing of Metals, Harbin Institute of Technology, Harbin 150001, Heilongjiang, China.
[#]These authors contributed equally to this work.

[*]**Correspondence to:** Dr. Bowen Bai, Dr. Jin Li, Dr. Xuesong Leng, Research Institute of Physical Sciences in Special Environments, Harbin Institute of Technology (Shenzhen), Shenzhen 518055, Guangdong, China. E-mail: baibowen@hit.edu.cn; lijin2019@hit.edu.cn; lengxuesong@hit.edu.cn

EXPERIMENTAL

Chemical Reagents

Trimethyl(methylcyclopentadienyl)platinum ($C_9H_{16}Pt$, AR grade) was purchased from Energy Chemical. Tin powder (Sn, 99.99%), potassium hydroxide (KOH, AR grade), and N,N-dimethylformamide (DMF, C_3H_7NO, 99.99%) were purchased from Aladdin Reagent (Shanghai) Co., Ltd. Commercial Pt/C (20 wt%) was purchased from Shanghai Hesen Electric Co., Ltd. Anhydrous ethanol (AR grade) was purchased from Sinopharm Chemical Reagent Co., Ltd. Nafion^{TM} perfluorinated resin solution (5 wt% in lower aliphatic alcohols and water, containing 45% water, Product No. 527084) and

sulfuric acid (H_2SO_4, ACS reagent, 95.0–98.0%, Product No. 320501) were obtained from Sigma-Aldrich. VULCAN® XC72R conductive carbon black was obtained from Cabot Corporation. Deionized water was used throughout the experiments. All reagents were used as received without further purification.

Synthesis of Sn NSs

Two-dimensional tin nanosheets (Sn NSs) were synthesized by a low-temperature liquid-phase exfoliation method under ice-bath conditions. Briefly, tin powder was first ground in an agate mortar for 30 min and then transferred into 100 mL of DMF. The resulting dispersion was subjected to probe ultrasonication in an ice bath at an ultrasonic power of 500 W using a pulsed mode with a pulse duration of 2 s for a total sonication time of 6 h. After ultrasonication, the dispersion was centrifuged at 3000 rpm for 5 min to remove unexfoliated bulk Sn. The supernatant was collected and further centrifuged at 11000 rpm for 10 min. The resulting Sn NSs were finally redispersed in DMF for subsequent Pt nanoparticle deposition. The centrifugation steps were performed using a high-speed centrifuge (TGL-15B, Shanghai Anting Scientific Instrument Factory, China).

Preparation of Pt/Sn NSs

The Pt/Sn NSs heterostructure was prepared by atomic layer deposition (ALD) using an atomic layer deposition system (D100-4882, Chongqing Nuotu Technology Co., Ltd., China). Typically, 15 mg of Sn NSs was uniformly dispersed on a heat-resistant quartz glass substrate with the assistance of anhydrous ethanol and then naturally dried at room temperature. The dried sample was transferred into the ALD chamber for Pt deposition.

During the ALD process, the chamber temperature was maintained at 250 °C. Trimethyl(methylcyclopentadienyl)platinum was used as the Pt precursor and heated to 65 °C, with N_2 used as the carrier and purge gas. Each ALD cycle consisted of Pt precursor exposure, reaction, purge, oxidant exposure, reaction, and purge steps. The Pt/Sn NSs catalyst used for subsequent studies was obtained after 60 ALD cycles. After deposition, the material was scraped from the quartz substrate and collected for further characterization and electrochemical measurements. To optimize the Pt loading, Pt/Sn NSs samples with different ALD cycles were also prepared.

Electrochemical Measurements

All electrochemical measurements were conducted at room temperature using an electrochemical workstation (CHI 760E, Shanghai Chenhua Instrument Co., Ltd., China) in a conventional three-electrode configuration. A catalyst-coated electrode was used as the working electrode, a high-purity graphite rod as the counter electrode, and a saturated calomel electrode (SCE) as the reference electrode. HER measurements were performed in 0.5 M H_2SO_4 and 1.0 M KOH aqueous solutions. All polarization curves were iR-corrected. The measured potentials were converted to the reversible hydrogen electrode (RHE) scale according to the following equation:

$$E_{RHE} = E_{SCE} + E_0 + 0.059 \times pH \quad (1)$$

where E_0 = 0.2438 V.

For HER measurements, 3 mg of catalyst and 2 mg of carbon black were dispersed in a mixed solution containing 490 μL of deionized water, 490 μL of ethanol, and 20 μL of Nafion solution. The mixture was homogenized using an ultrasonic cleaner (K3200DE, Kunshan Ultrasonic Instruments Co., Ltd., China) to obtain a homogeneous catalyst ink. Subsequently, 2 μL of the catalyst ink was uniformly deposited onto the surface of the working electrode. The corresponding reference catalysts were prepared using the same procedure.

The HER activity was evaluated by linear sweep voltammetry (LSV). In 0.5 M H_2SO_4, HER measurements were performed in an iR-corrected standard three-electrode system at a scan rate of 5 mV s^{-1}. The alkaline HER performance of Pt/Sn NSs was also evaluated in 1.0 M KOH. The Tafel slope was derived from the corresponding polarization curve according to the Tafel equation:

$$\eta = b\log j + a \quad (2)$$

where η is the overpotential, j is the current density, b is the Tafel slope, and a is a constant. The mass activity of the Pt-based catalysts was normalized to the actual mass of Pt loaded on the working electrode. The Pt content in Pt/Sn NSs was quantitatively determined by inductively coupled plasma optical emission spectroscopy (ICP-OES, Agilent 5110, Agilent Technologies, USA) and was measured to be 13.6 wt%, which was subsequently used for calculating the Pt-mass-normalized catalytic activity.

To assess the relative electrochemically accessible surface area of the catalysts, electrochemical double-layer capacitance (Cdl) was determined from cyclic voltammetry (CV) measurements in a non-Faradaic potential region. CV curves were recorded in both 0.5 M H_2SO_4 and 1.0 M KOH at scan rates of 20, 40, 60, 80, and 100 mV s^{-1}. The C_{dl} values were obtained from the linear relationship between the capacitive current response and the scan rate.

Electrochemical impedance spectroscopy (EIS) was employed to investigate the interfacial charge-transfer behavior of Pt/Sn NSs and commercial 20 wt% Pt/C. EIS measurements were conducted in both 0.5 M H_2SO_4 and 1.0 M KOH, and the charge-transfer resistance of the catalysts was evaluated from the corresponding Nyquist plots.

The electrochemical stability of Pt/Sn NSs was evaluated by chronoamperometric measurements under constant applied potentials in both 0.5 M H_2SO_4 and 1.0 M KOH for 30 h, with current density recorded as a function of time. In addition, cycling stability was assessed by CV cycling tests, and the LSV curves of Pt/Sn NSs and commercial 20 wt% Pt/C were compared before and after 2000 CV cycles in both electrolytes.

Characterization

The principal characterization methods are described in the “Material characterization” subsection of the main manuscript. Briefly, SEM/EDS measurements were performed using a JSM-6700 scanning electron microscope (JEOL Ltd., Japan); TEM characterization was conducted using a JEM-F200 transmission electron microscope (JEOL Ltd., Japan) at 200 kV; XRD measurements were performed using a Y-2000 diffractometer (Dandong Aolong Radiative Instrument Co., Ltd., China); XPS measurements were conducted using an ESCALAB 250 Xi spectrometer (Thermo Fisher Scientific, United Kingdom); and the Pt content was determined by ICP-OES (Agilent 5110, Agilent Technologies, USA), giving a Pt mass fraction of 13.6 wt%.

DFT Calculations

Density functional theory (DFT) calculations were performed to investigate the Pt-

support interaction, electronic structure, adsorption behavior, and HER reaction energetics of Pt/Sn NSs and Pt/C. Structural models of Pt/Sn NSs and Pt/C were constructed, and the corresponding reaction intermediates involved in acidic and alkaline HER pathways were considered.

The binding energy between Pt species and the corresponding support was calculated to evaluate the strength of Pt-support interaction. Charge-density-difference analysis, plane-averaged charge-density-difference profiles Δρ(z), and Bader charge analysis were used to examine interfacial charge redistribution and quantify charge transfer. Density of states (DOS) and Pt d-band centers were calculated to analyze support-induced modulation of the Pt electronic structure. The adsorption energies of H* and H_2O were calculated to evaluate the interaction between key HER intermediates and active sites.

The Gibbs free-energy change was obtained from:

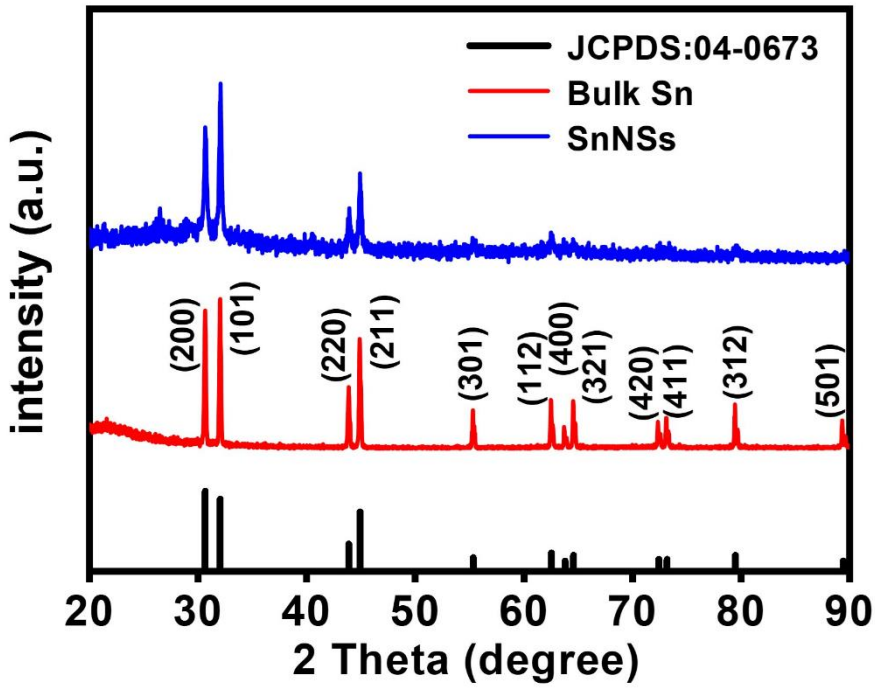
$$\Delta G = \Delta E + \Delta ZPE - T\Delta S \quad (3)$$

where ΔE is the DFT electronic-energy change, ΔZPE is the zero-point-energy correction, and ΔS is the entropy change at the calculation temperature. For acidic HER, the key hydrogen-adsorption free energy is:

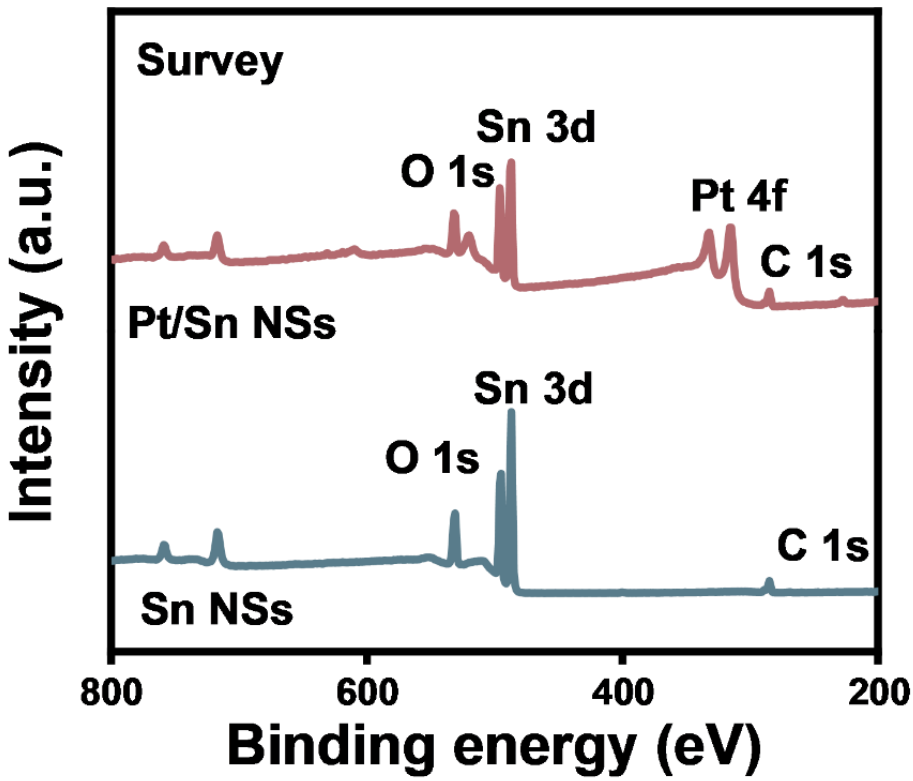
$$\Delta G(H^*) - G(^*) - 1/2\, G(H_2) \quad (4)$$

A ΔG(H*) value close to 0 eV indicates thermodynamically favorable H* adsorption/desorption. For alkaline HER, H_2O adsorption/dissociation and subsequent H* formation/H_2 evolution steps were considered to compare the reaction energetics of Pt/Sn NSs and Pt/C.

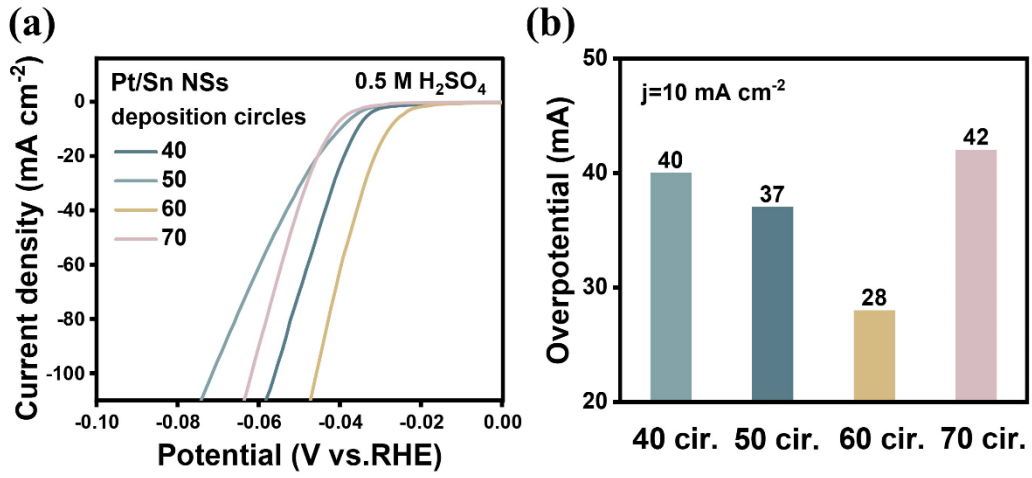
The ΔG values discussed herein represent thermodynamic Gibbs free-energy changes between the corresponding reaction states and should not be interpreted as kinetic activation barriers. No transition-state or nudged elastic band calculations were performed in the present work.



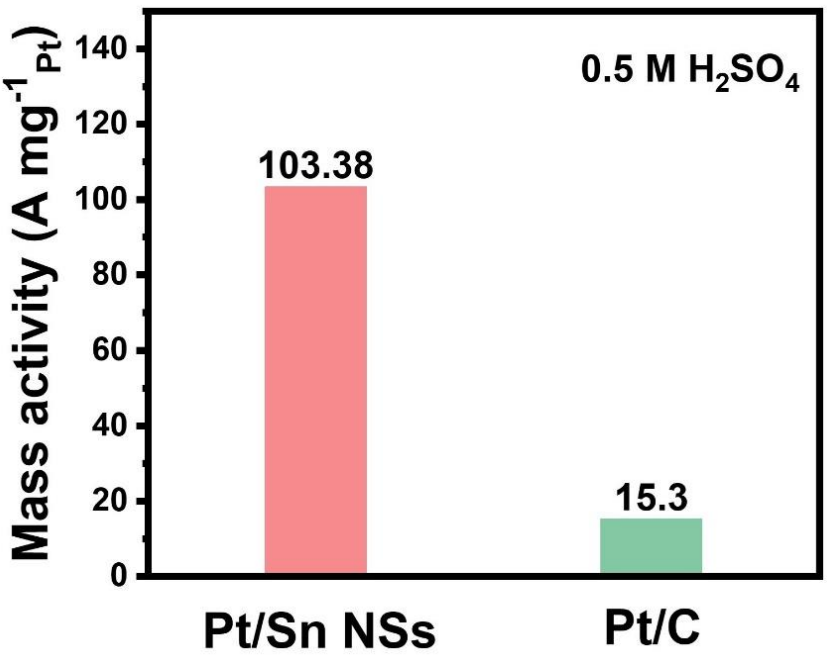
Supplementary Figure 1. XRD patterns of Bulk Sn and Sn NSs.



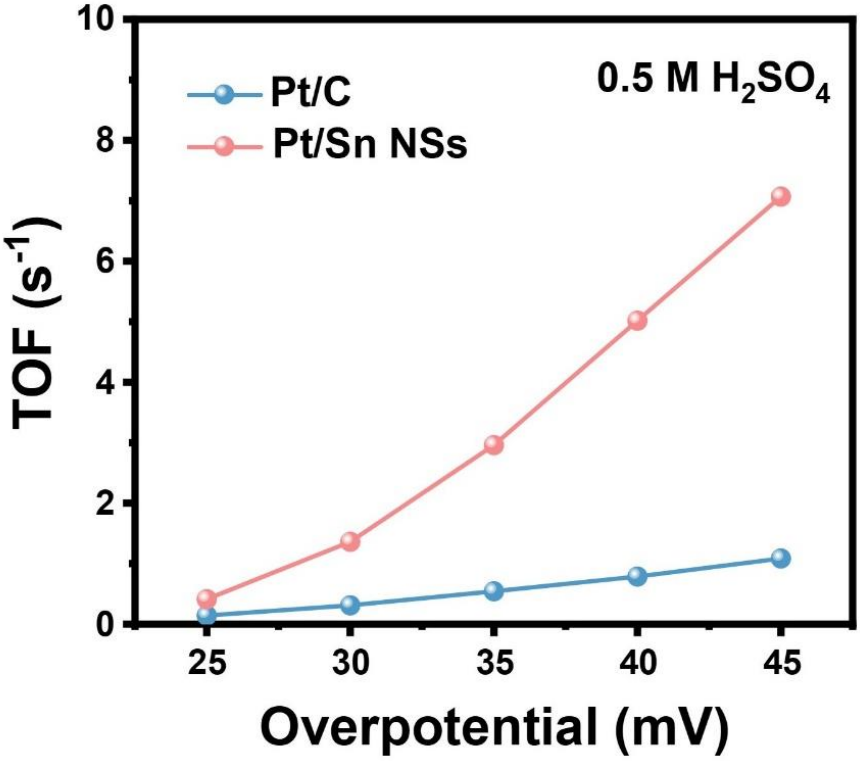
Supplementary Figure 2. The XPS spectra of Sn NSs and Pt/Sn NSs.



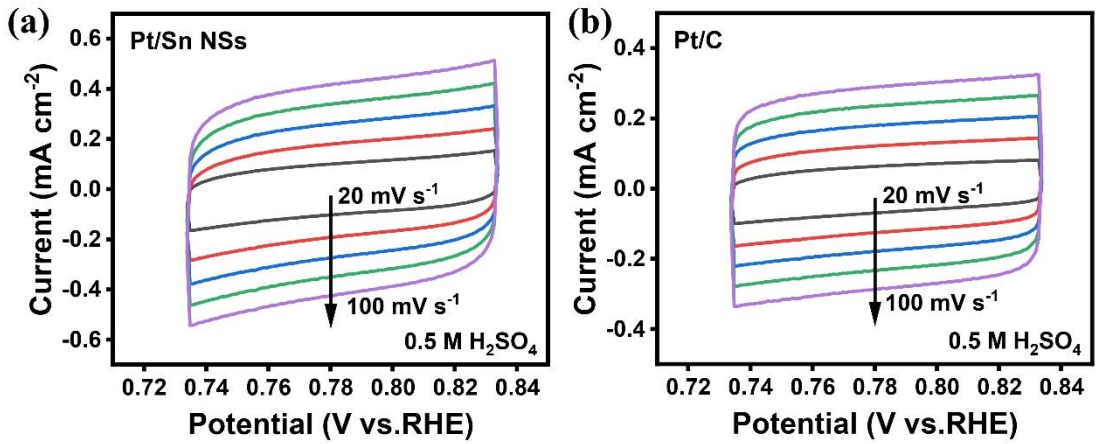
Supplementary Figure 3. Optimization of Pt loading on Sn NSs. (a) HER polarization curves of Pt/Sn NSs prepared with different ALD Pt deposition cycles in 0.5 M H_2SO_4. (b) Comparison of overpotentials at a current density of 10 mA cm^{-2}.



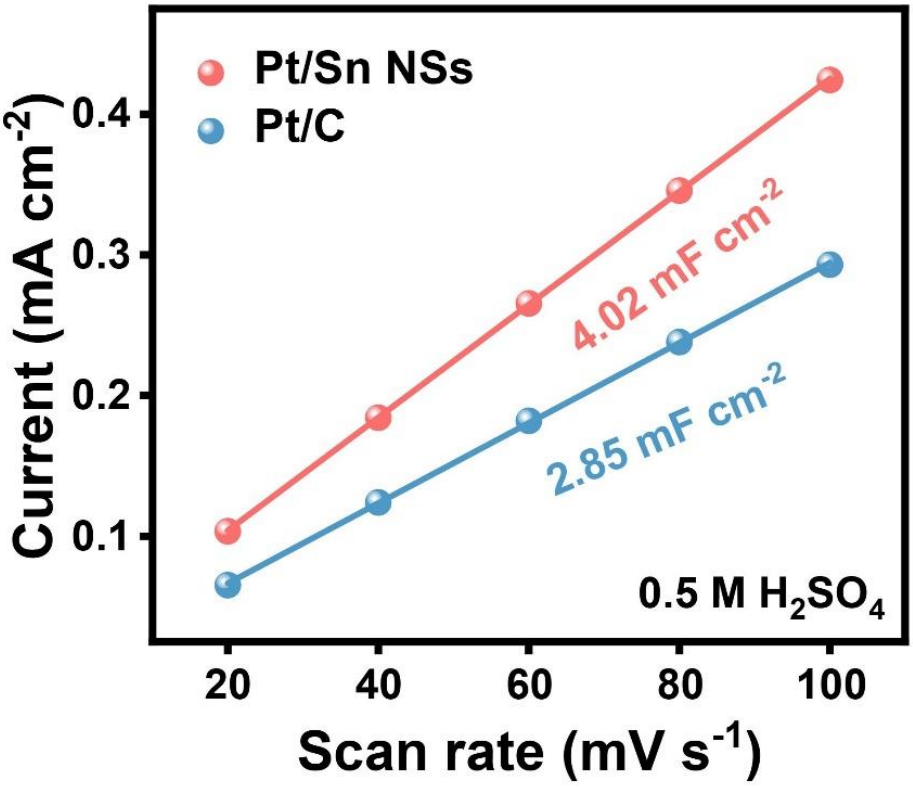
Supplementary Figure 4. Pt-mass-normalized HER activity of Pt/Sn NSs and commercial 20 wt% Pt/C in 0.5 M H_2SO_4.



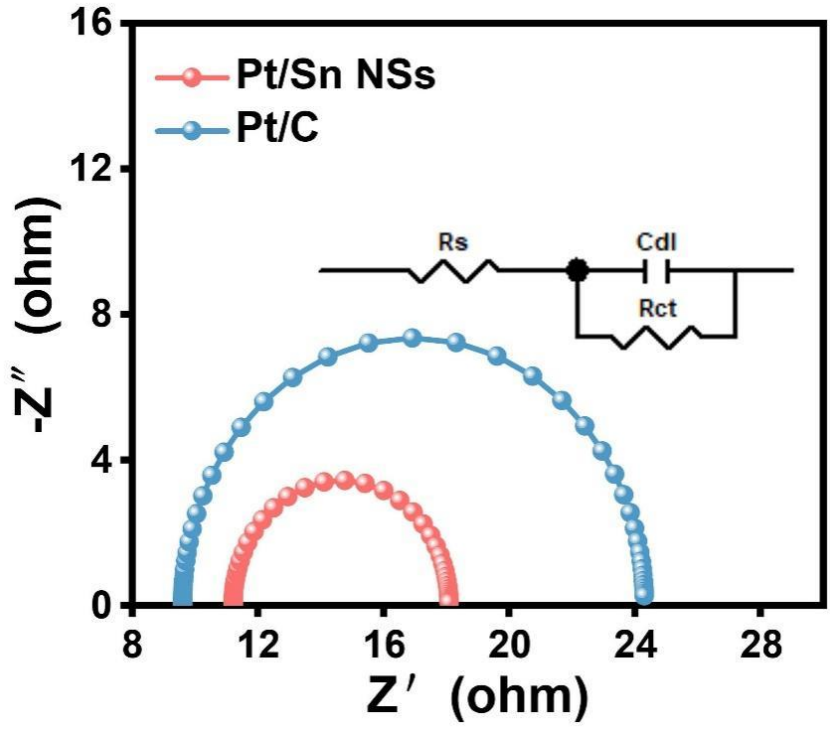
Supplementary Figure 5. Turnover frequency (TOF) comparison of Pt/Sn NSs and commercial 20 wt% Pt/C in 0.5 M H_2SO_4.



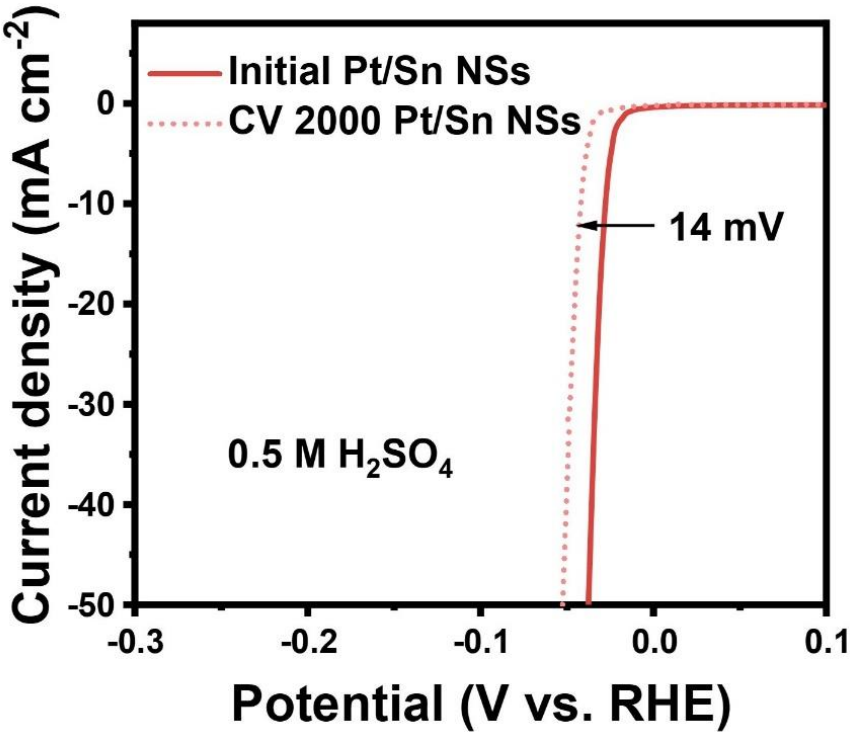
Supplementary Figure 6. CV curves of (a) Pt/Sn NSs and (b) commercial 20 wt% Pt/C recorded in the non-Faradaic region at different scan rates (20, 40, 60, 80, and 100 mV s^{-1}) in 0.5 M H_2SO_4.



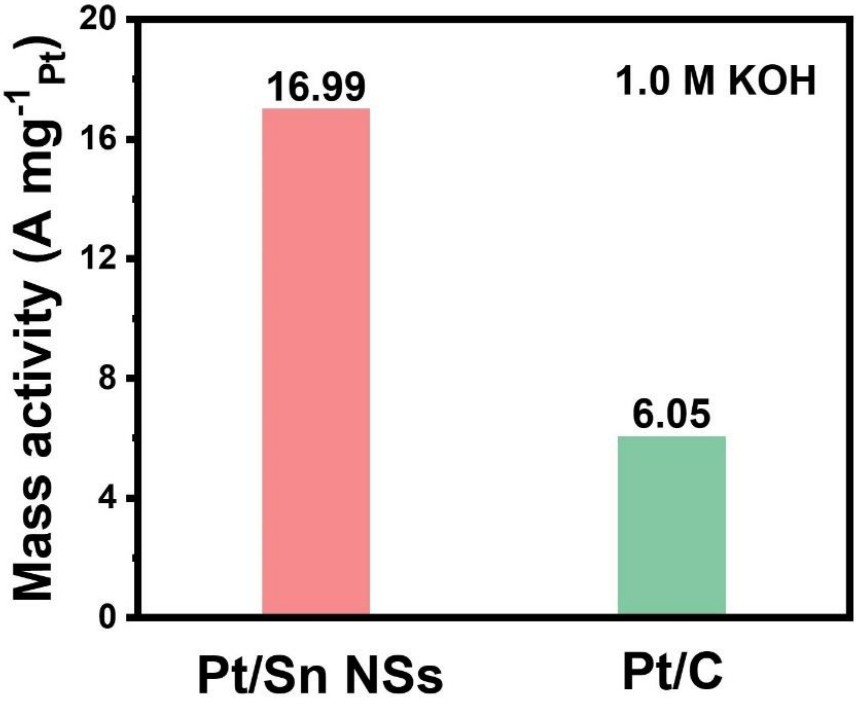
Supplementary Figure 7. Double-layer capacitance (Cdl) measurements of Pt/Sn NSs and commercial 20 wt% Pt/C in 0.5 M H_2SO_4.



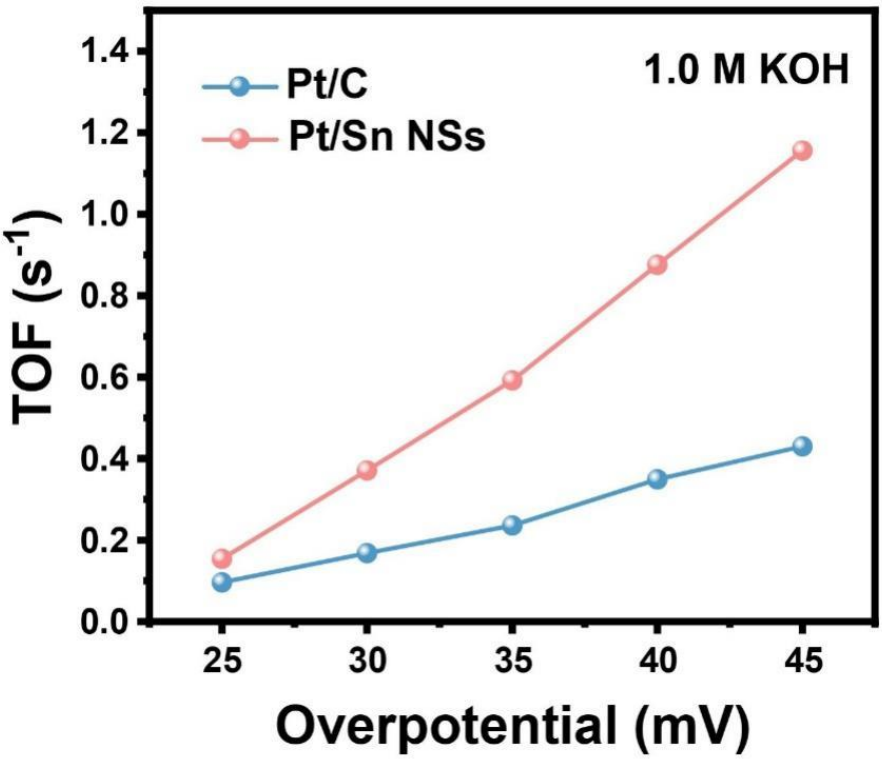
Supplementary Figure 8. Electrochemical impedance spectra of Pt/Sn NSs and commercial 20 wt% Pt/C in 0.5 M H_2SO_4.



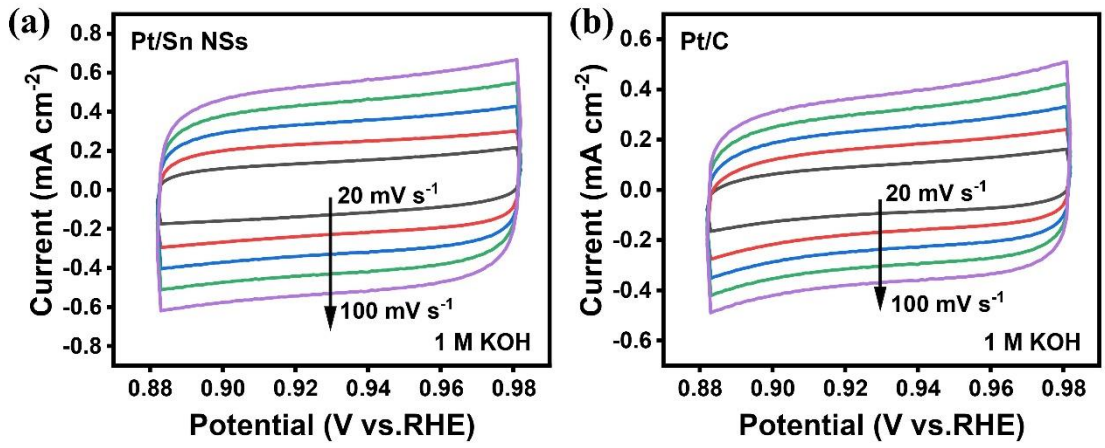
Supplementary Figure 9. Comparison of the initial and post-2000-cycle HER polarization curves of Pt/Sn NSs in 0.5 M H_2SO_4.



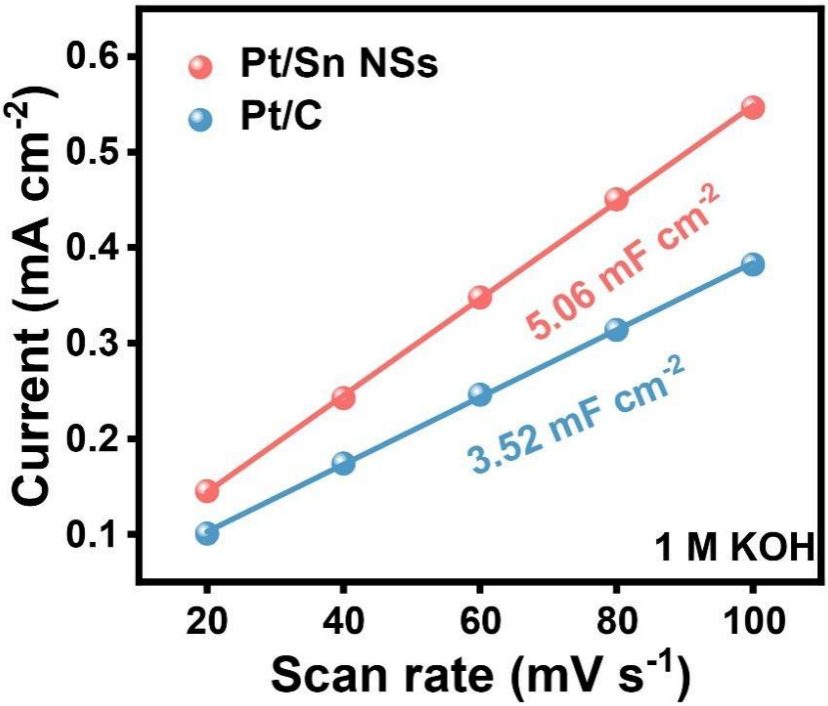
Supplementary Figure 10. The mass activity of Pt/Sn NSs and 20 wt% Pt/C in 1.0 M KOH.



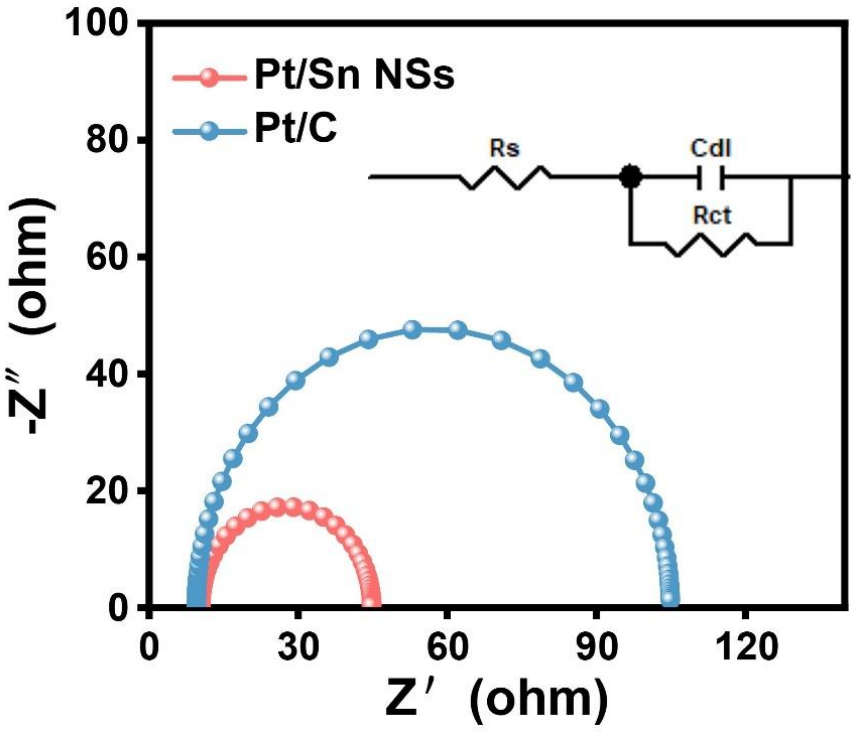
Supplementary Figure 11. Turnover frequency (TOF) of Pt/Sn NSs and 20 wt% Pt/C in 1.0 M KOH.



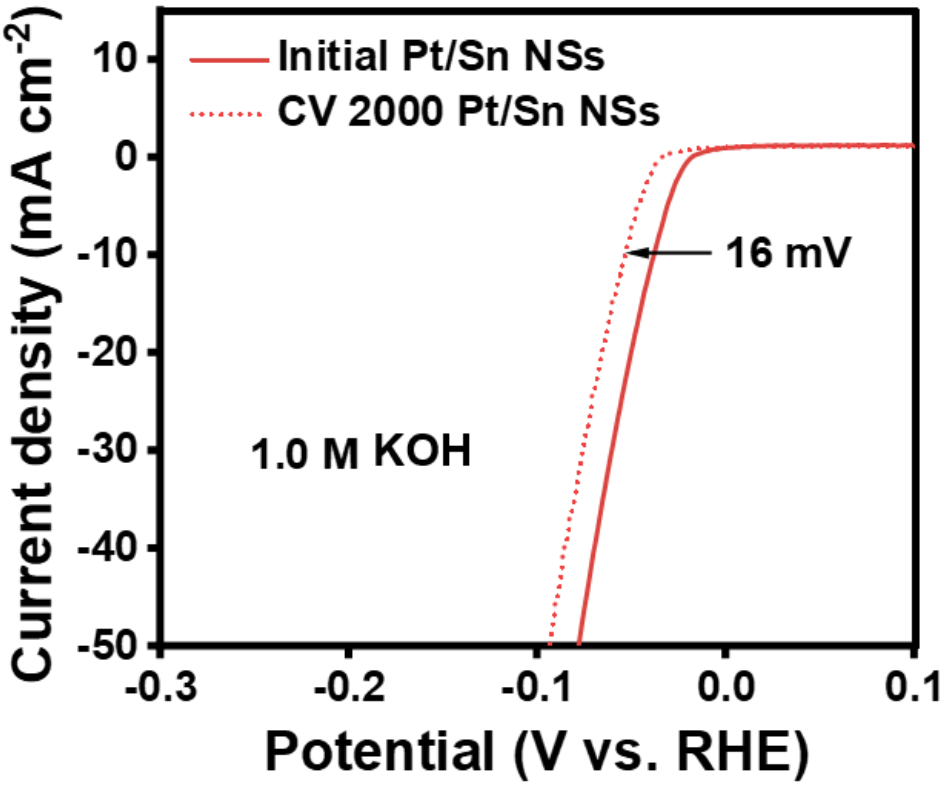
Supplementary Figure 12. CV curves of (a) Pt/Sn NSs and (b) commercial 20 wt% Pt/C recorded in the non-Faradaic region at scan rates of 20, 40, 60, 80, and 100 mV s^{-1} in 1.0 M KOH.



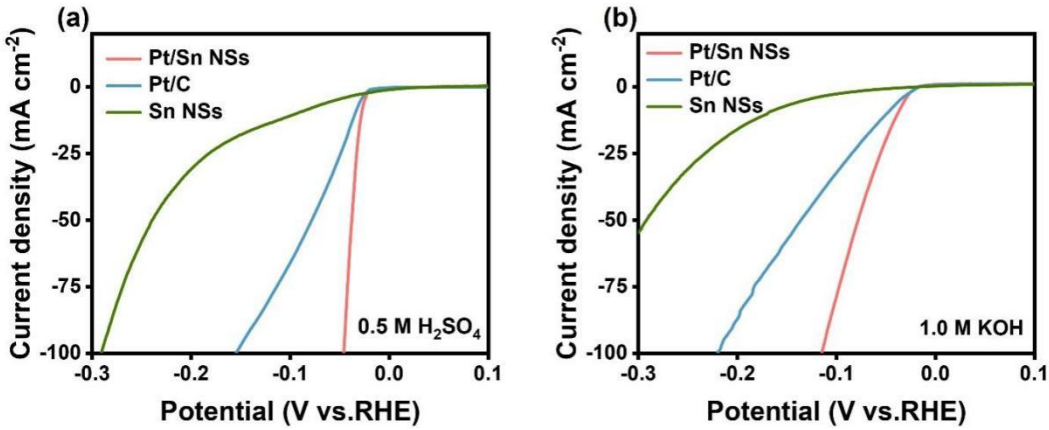
Supplementary Figure 13. The double-layer capacitance of Pt/Sn NSs and 20 wt% Pt/C in 1.0 M KOH.



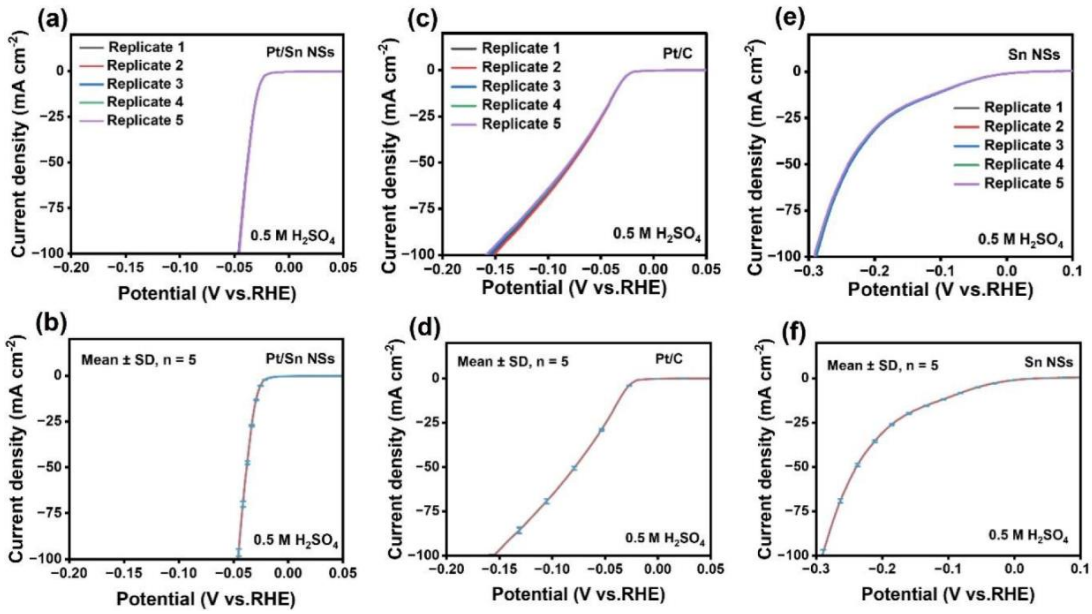
Supplementary Figure 14. Electrochemical impedance spectroscopy test of Pt/Sn NSs and 20 wt% Pt/C in 1.0 M KOH.



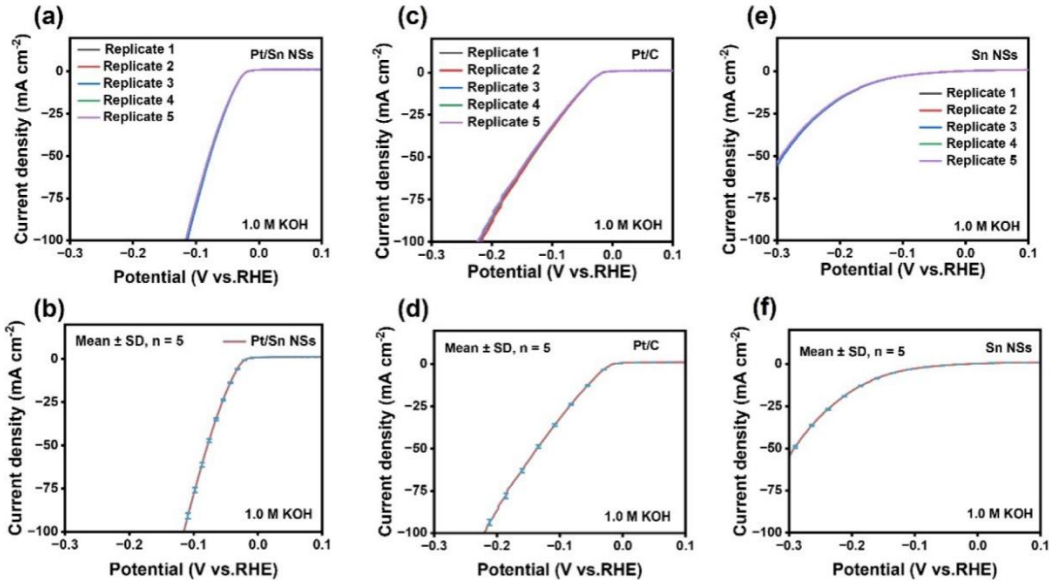
Supplementary Figure 15. Comparison of the initial and post-2000-cycle HER polarization curves of Pt/Sn NSs in 1.0 M KOH.



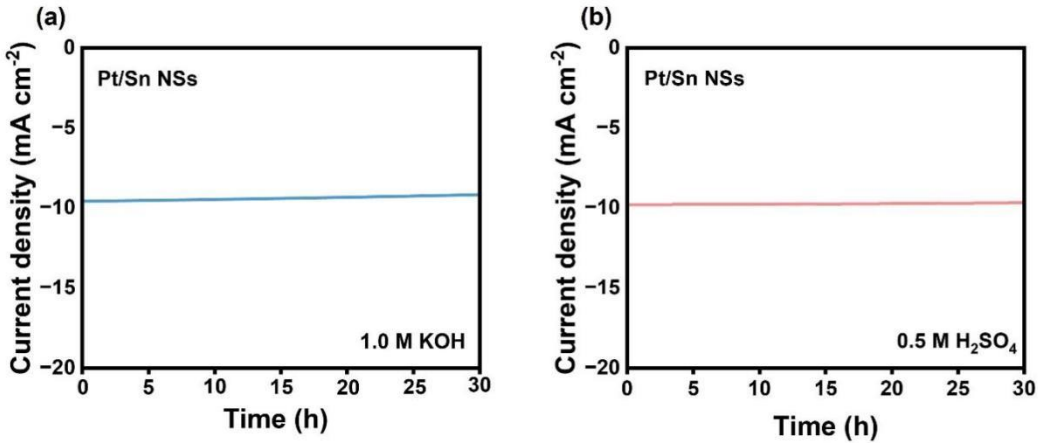
Supplementary Figure 16. HER performance comparison of bare Sn NSs, Pt/Sn NSs, and commercial Pt/C. (a) HER polarization curves in 0.5 M H_2SO_4. (b) HER polarization curves in 1.0 M KOH.



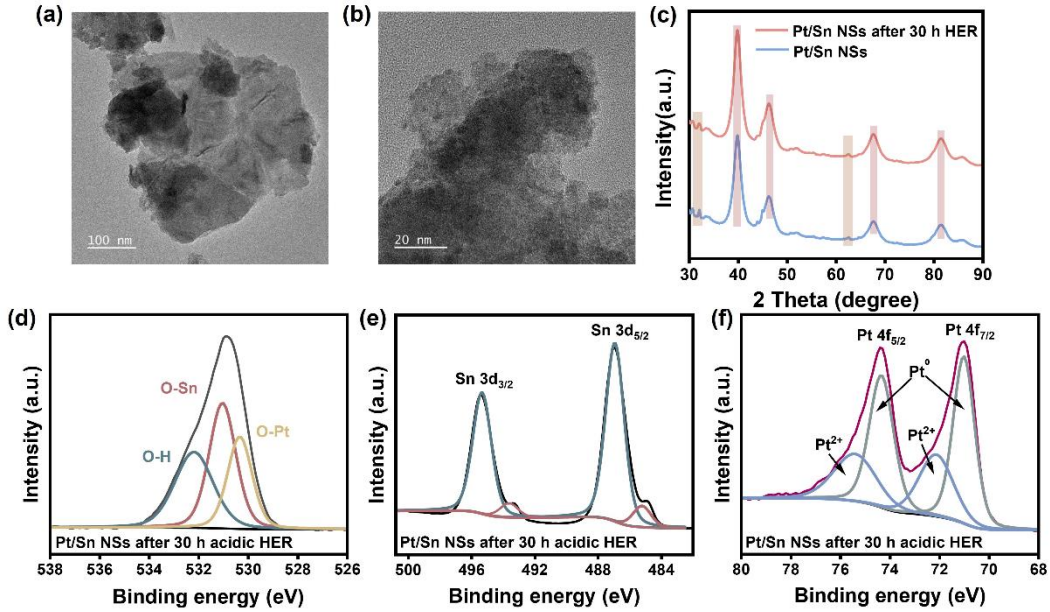
Supplementary Figure 17. Reproducibility evaluation of HER polarization curves for Pt/Sn NSs, commercial Pt/C, and bare Sn NSs in 0.5 M H_2SO_4 based on five independent measurements. (a, c, e) Individual HER polarization curves of Pt/Sn NSs, commercial Pt/C, and bare Sn NSs, respectively, obtained from five repeated measurements. (b, d, f) Averaged polarization curves with standard deviations (mean ± SD, n = 5) corresponding to Pt/Sn NSs, commercial Pt/C, and bare Sn NSs, respectively.



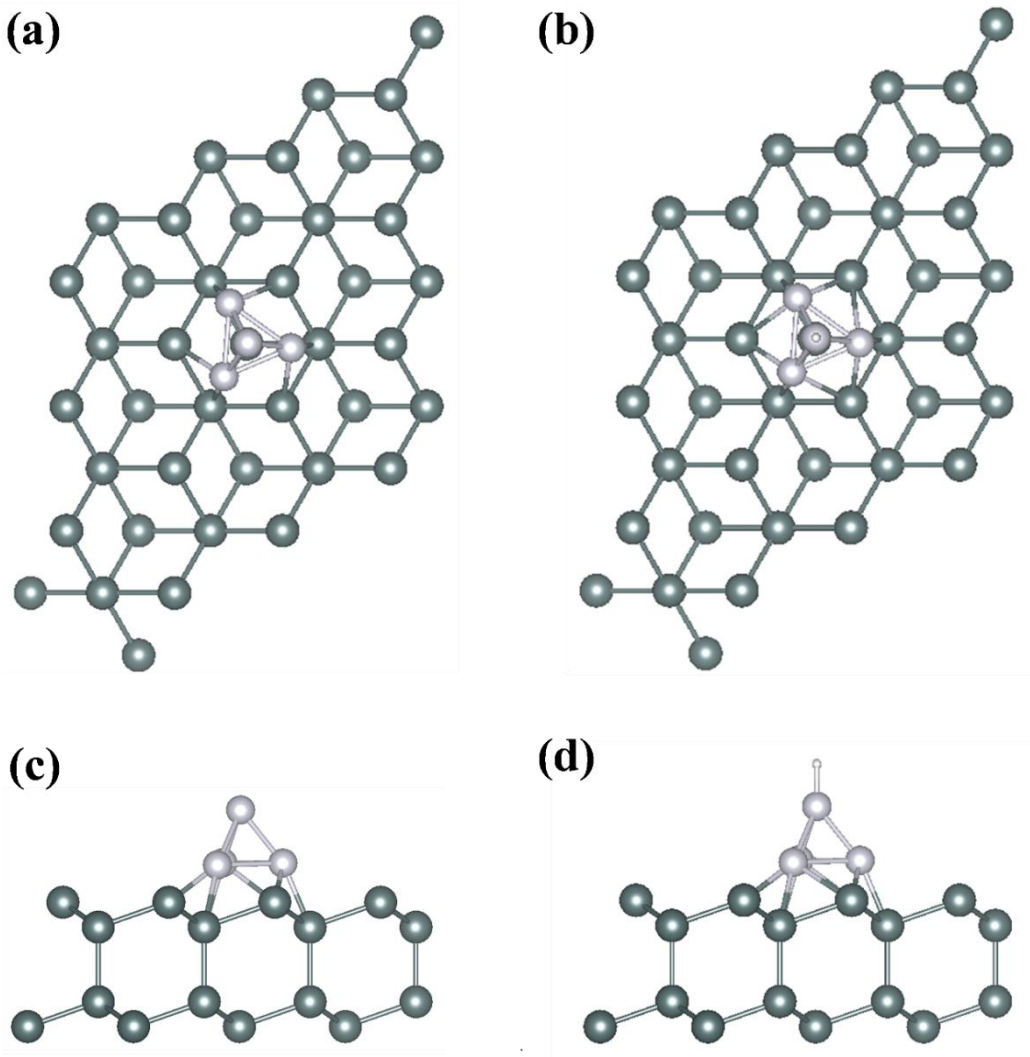
Supplementary Figure 18. Reproducibility evaluation of HER polarization curves for Pt/Sn NSs, commercial Pt/C, and bare Sn NSs in 1.0 M KOH based on five independent measurements. (a, c, e) Individual HER polarization curves of Pt/Sn NSs, commercial Pt/C, and bare Sn NSs, respectively, obtained from five repeated measurements. (b, d, f) Averaged polarization curves with standard deviations (mean ± SD, n = 5) corresponding to Pt/Sn NSs, commercial Pt/C, and bare Sn NSs, respectively.



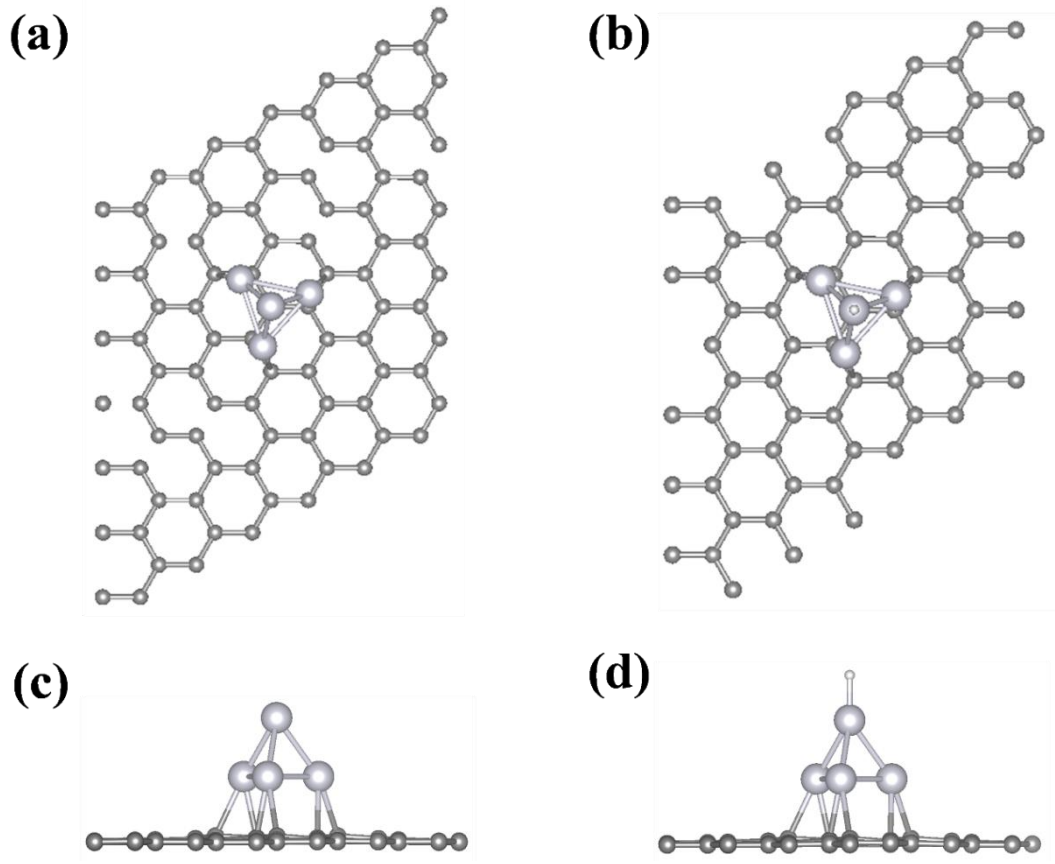
Supplementary Figure 19. Long-term chronoamperometric stability tests of Pt/Sn NSs under constant applied potentials for 30 h in (a) 1.0 M KOH and (b) 0.5 M H_2SO_4.



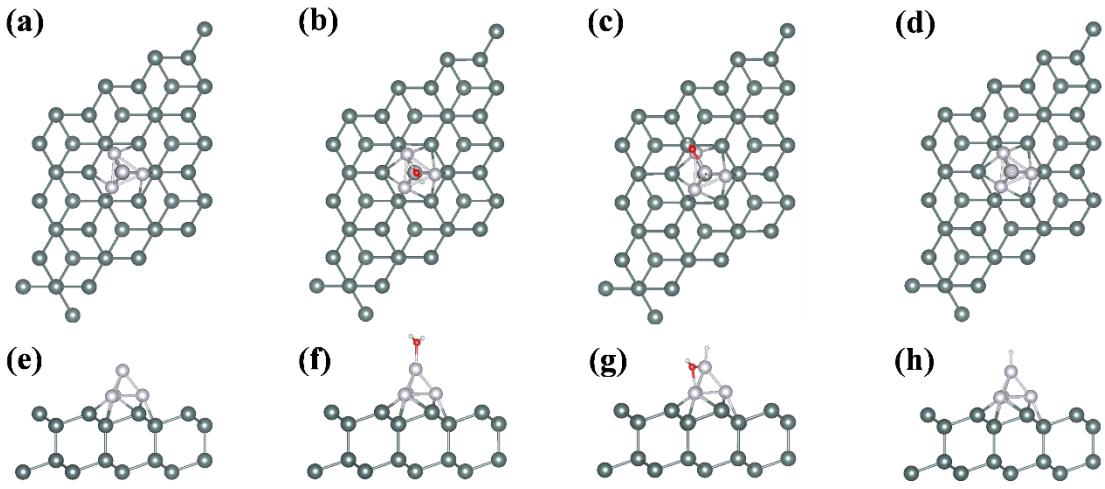
Supplementary Figure 20. Structural and surface-chemical characterization of Pt/Sn NSs after 30 h of HER operation in 0.5 M H_2SO_4. (a, b) TEM images of Pt/Sn NSs after the stability test at different magnifications. (c) XRD patterns of Pt/Sn NSs before and after the stability test. (d–f) High-resolution O 1s, Sn 3d, and Pt 4f XPS spectra, respectively, of Pt/Sn NSs after the stability test.



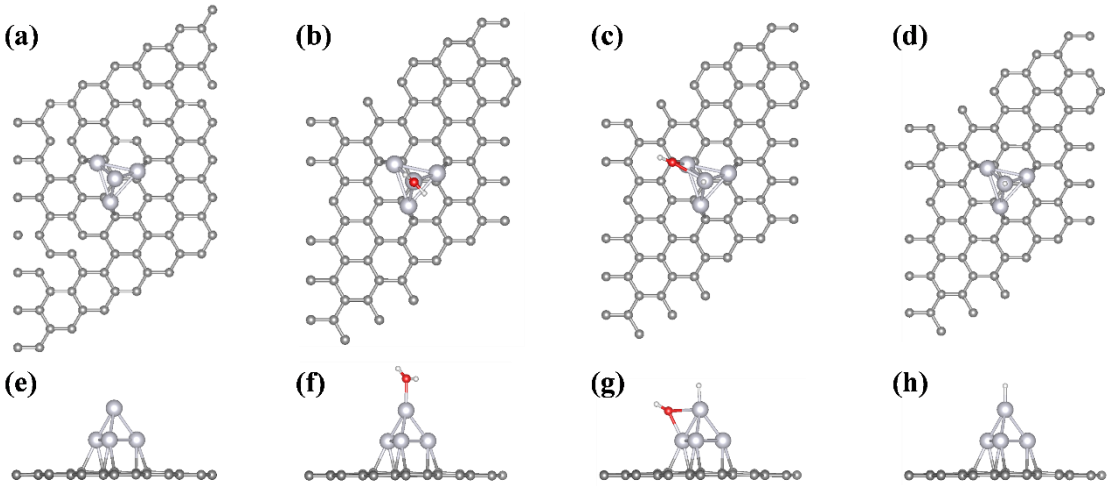
Supplementary Figure 21. Structure models and chemisorption configuration models for Pt/Sn NSs. Top view (a), side view (c) of structure models, and the corresponding (b, d) H*Pt/Sn NSs intermediate adsorption configurations for acidic HER.



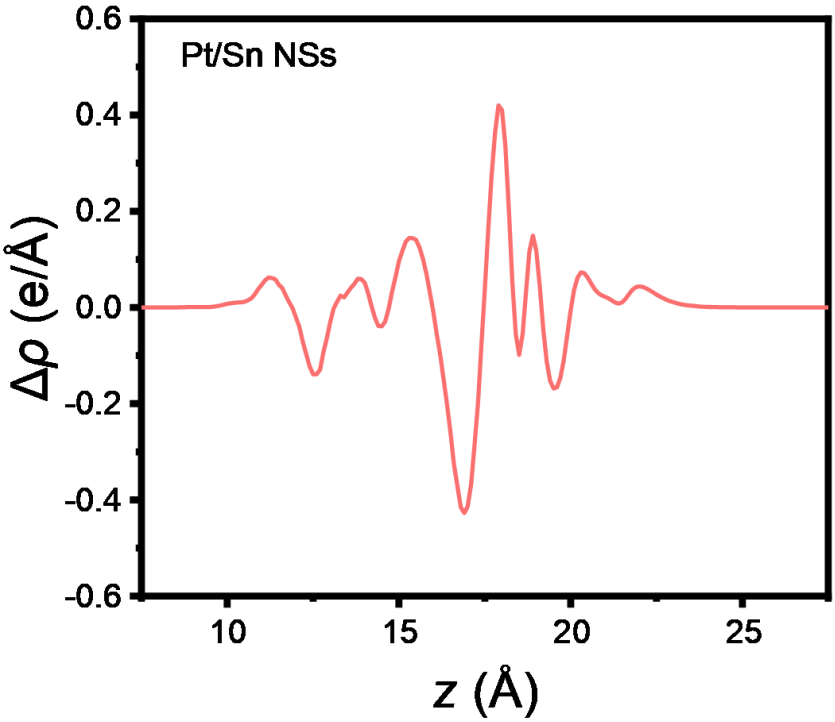
Supplementary Figure 22. Structure models and chemisorption configuration models for Pt/C. Top view (a), side view (c) of structure models, and the corresponding (b, d) H*Pt/C intermediate adsorption configurations for acidic HER.



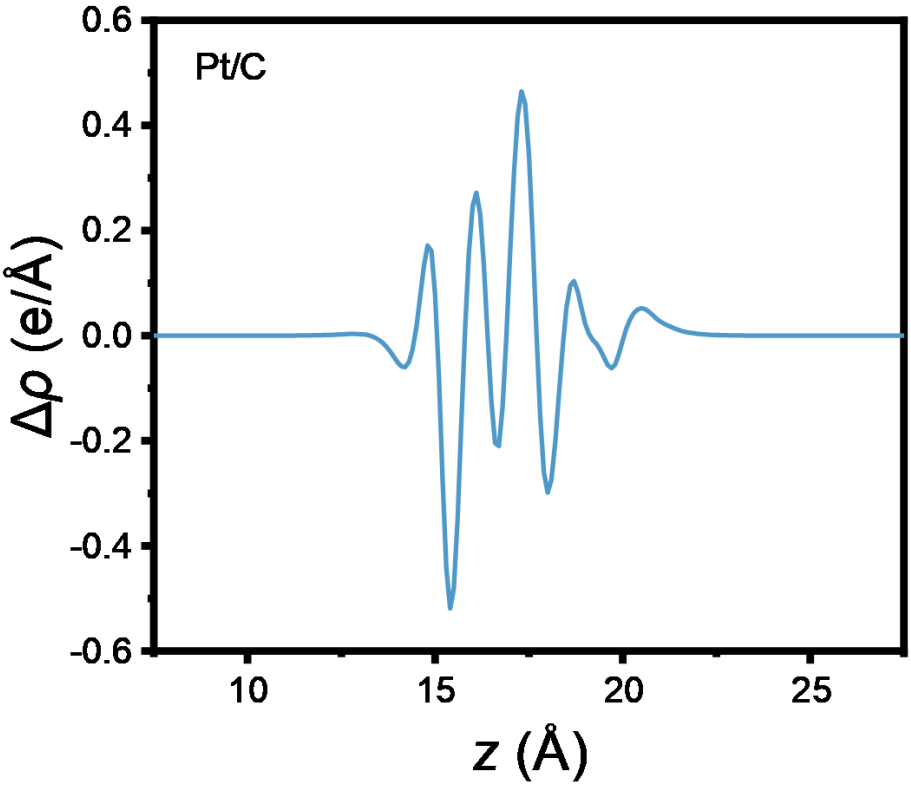
Supplementary Figure 23. Structural model and adsorption configurations of Pt/Sn NSs for alkaline HER. (a, e) Top and side views of the structural model, respectively. (b, f) H_2O* adsorption configurations; (c, g) H* + OH* co-adsorption configurations; (d, h) H* adsorption configurations.



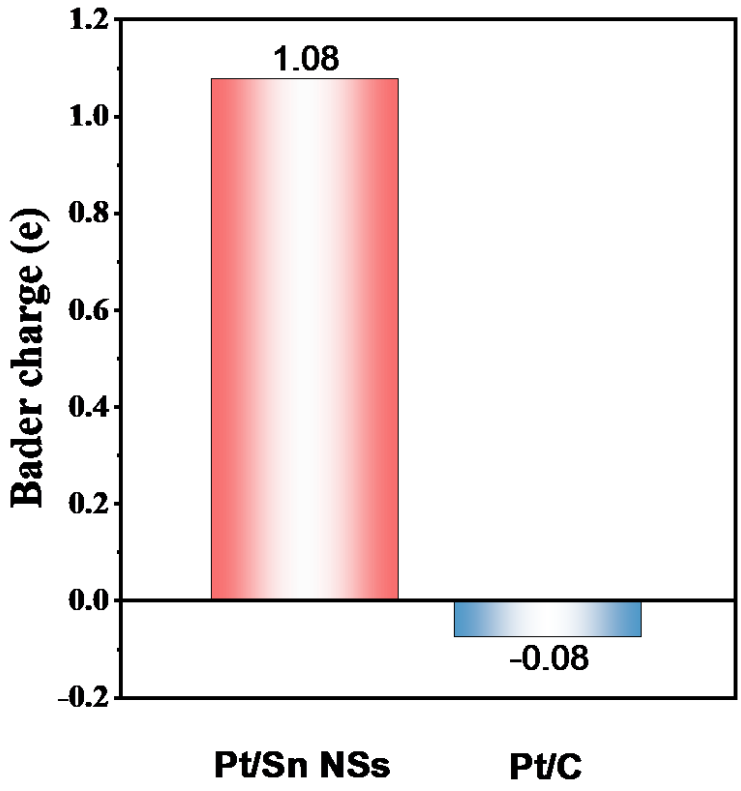
Supplementary Figure 24. Structural model and adsorption configurations of Pt/C for alkaline HER. (a, e) Top and side views of the structural model, respectively. (b, f) H_2O* adsorption configurations; (c, g) H* + OH* co-adsorption configurations; (d, h) H* adsorption configurations.



Supplementary Figure 25. Planar-averaged charge-density difference, Δρ(z), along the z direction for Pt/Sn NSs.



Supplementary Figure 26. Planar-averaged charge-density difference, Δρ(z), along the z direction for Pt/C.



Supplementary Figure 27. Bader charge comparison of Pt/Sn NSs and Pt/C.

Supplementary Table 1. Quantitative ICP-OES determination of Pt content in Pt/Sn NSs

Test element	Percentage content (wt %)
Pt	13.6

Supplementary Table 2. Comparison of the HER performance of Pt/Sn NSs with reported catalysts in 0.5 M H_2SO_4

Catalysts	η_{10}(mV)	Tafel slope (mV dec^{-1})	Ref.
Ni-Pt films	90	49	[1]
10Pt/VS_2/CP	77	39.46	[2]
S-M-5Pt	62	78	[3]
Pt_1@Fe-N-C	60	42	[4]
Pt-SA/m-WO_{3-x}	47	45	[5]
$Pt_{56}Fe_{44}$	45	22	[6]
Pt_3Co@NCNT	42	27.20	[7]
Pt/CNT45	41	17	[8]
Pt/$RuCeO_x$-PA	41	31	[9]
Pt@C_2N	40	33	[10]
Pt/Sn NSs	28	13.5	This work

Supplementary Table 3. Comparison of the HER performance of Pt/Sn NSs with reported catalysts in 1.0 M KOH

Catalysts	η_{10} (mV)	Tafel slope (mV dec^{-1})	Ref.
Pt_1@Co/NC	305	151	[11]
Pt@PCM	139	73.6	[12]
SA-Pt/MoS_2	123	76.71	[13]
Pt@NiFe LDHs	101	127	[14]
Pt-AC/DG-4	97	56.50	[15]
Pt-NiCo LDO	92	73	[16]
$RhSe_2$	81.6	96	[17]
Pt/CNT45	74	70	[8]
Pt_{SA}-$NiMoO_4 \cdot xH_2O$	73	155	[18]
Pt-V_2CT_X	68.1	98.6	[19]

Pt/Sn NSs	37	35.7	This work

Supplementary Table 4. Linear regression parameters for the apparent Tafel slopes of Pt/Sn NSs and commercial Pt/C in acidic and alkaline electrolytes

Electrolyte	Catalyst	Fitting range (mA cm^{-2})	Intercept (mV)	Apparent Tafel slope (mV dec^{-1})	R^2
0.5 M H_2SO_4	Pt/Sn NSs	10.81–42.06	14.02316	13.47473	0.99590
0.5 M H_2SO_4	Pt/C	4.77-10.86	14.76321	19.47731	0.99502
1.0 M KOH	Pt/Sn NSs	7.20-19.07	2.63021	35.65670	0.99231
1.0 M KOH	Pt/C	6.91-16.93	-15.55374	65.23844	0.98872

The fits were performed using unweighted linear least-squares regression in Origin according to $\eta = a + bx$, where η is the overpotential in mV, a is the intercept, b is the apparent Tafel slope in mV dec^{-1}, and $x = \log_{10}(|j|/[\text{mA cm}^{-2}])$. The fitting range denotes the current-density interval used for each regression, and R^2 is the coefficient of determination.

Supplementary Table 5. Tabulated coordinates of the linear fits to the HER Tafel data for Pt/Sn NSs and commercial Pt/C in 0.5 M H_2SO_4

Pt/Sn NSs: x	Pt/Sn NSs:η_{fit} (mV)	Pt/C: x	Pt/C:η_{fit} (mV)
1.03376	27.95285	0.67839	27.97639
1.09933	28.83630	0.71808	28.74951
1.16489	29.71974	0.75778	29.52262
1.23045	30.60319	0.79747	30.29574
1.29602	31.48663	0.83716	31.06885
1.36158	32.37008	0.87685	31.84197
1.42714	33.25352	0.91655	32.61508
1.49271	34.13697	0.95624	33.38819
1.55827	35.02041	0.99593	34.16131
1.62383	35.90386	1.03563	34.93442

Here, x = $\log_{10}(|j|/[\text{mA cm}^{-2}])$, and η_{fit} is the fitted overpotential in mV. The tabulated values are coordinates of the fitted lines, rather than additional experimental measurements.

Supplementary Table 6. Tabulated coordinates of the linear fits to the HER Tafel data for Pt/Sn NSs and commercial Pt/C in 1.0 M KOH.

Pt/Sn NSs: x	**Pt/Sn NSs:η_{fit} (mV)**	**Pt/C: x**	**Pt/C:η_{fit} (mV)**
0.85742	33.20289	0.83956	39.21770
0.90441	34.87853	0.88279	42.03809
0.95140	36.55417	0.92602	44.85848
0.99840	38.22981	0.96925	47.67887
1.04539	39.90545	1.01249	50.49926
1.09239	41.58109	1.05572	53.31965
1.13938	43.25672	1.09895	56.14004
1.18637	44.93236	1.14218	58.96043
1.23337	46.60800	1.18541	61.78083
1.28036	48.28364	1.22865	64.60122

Here, x = $\log_{10}(|j|/[\text{mA cm}^{-2}])$, and η_{fit} is the fitted overpotential in mV. The tabulated values are coordinates of the fitted lines, rather than additional experimental measurements.

REFERENCES

[1] Eiler, K., S. Suriñach, J. Sort, et al. Mesoporous Ni-rich Ni–Pt thin films: electrodeposition, characterization and performance toward hydrogen evolution reaction in acidic media, *Appl. Catal. B-Environ. energy*, 2020, **265**, 118597. 10.1016/j.apcatb.2020.118597

[2] Zhu, J., L. Cai, X. Yin, et al. Enhanced electrocatalytic hydrogen evolution activity in single-atom Pt-decorated VS_2 nanosheets, *ACS Nano*, 2020, **14**(5), 5600-5608. 10.1021/acsnano.9b10048

[3] Cui, C., R. Cheng, H. Zhang, et al. Ultrastable MXene@Pt/SWCNTs' nanocatalysts for hydrogen evolution reaction, *Adv. Funct. Mater.*, 2020, **30**(47), 2000693. 10.1002/adfm.202000693

[4] Zeng, X., J. Shui, X. Liu, et al. Single-atom to single-atom grafting of Pt_1 onto Fe-N_4 Center: Pt_1@Fe-N-C multifunctional electrocatalyst with significantly enhanced properties, *Adv. Energy Mater.*, 2017, **8**(1), 1701345. 10.1002/aenm.201701345

[5] Park, J., S. Lee, H. E. Kim, et al. Investigation of the support effect in atomically dispersed Pt on WO_{3-x} for utilization of Pt in the hydrogen evolution reaction, *Angew. Chem. Int. Edit.*, 2019, **58**(45), 16038-16042. 10.1002/anie.201908122

[6] Li, Q., H. Zhu, X. Chen, et al. Local structure insight into hydrogen evolution reaction with bimetal nanocatalysts, *J. Am. Chem. Soc.*, 2022, **144**(44), 20298-20305. 10.1021/jacs.2c07844

[7] Zhang, S. L., X. F. Lu, Z. P. Wu, et al. Engineering platinum–cobalt nano-alloys in porous nitrogen-doped carbon nanotubes for highly efficient electrocatalytic hydrogen evolution, *Angew. Chem. Int. Edit.*, 2021, **60**(35), 19068-19073. 10.1002/anie.202106547

[8] Liu, Y., P. Liu, Y. Cai, et al. Platinum/(carbon-nanotube) electrocatalyst boosts hydrogen evolution reaction in acidic, neutral and alkaline solutions, *Small*, 2025, **21**, 2411181. 10.1002/smll.202411181

[9] Liu, T., W. Gao, Q. Wang, et al. Selective loading of atomic platinum on a $RuCeO_x$ support enables stable hydrogen evolution at high current densities, *Angew. Chem. Int.*

Edit., 2020, **59**(46), 20423-20427. 10.1002/anie.202009612

[10] Mahmood, J., F. Li, S.-M. Jung, et al. An efficient and pH-universal ruthenium-based catalyst for the hydrogen evolution reaction, *Nat. Nanotechnol.*, 2017, **12**(5), 441-446. 10.1038/nnano.2016.304

[11] Lai, W. H., L. F. Zhang, W. B. Hua, et al. General π-electron-assisted strategy for Ir, Pt, Ru, Pd, Fe, Ni single-atom electrocatalysts with bifunctional active sites for highly efficient water splitting, Angew. Chem. Int. Ed., 2019, 58(34), 11868-11873. 10.1002/anie.201904614

[12] Zhang, H., P. An, W. Zhou, et al. Dynamic traction of lattice-confined platinum atoms into mesoporous carbon matrix for hydrogen evolution reaction, Sci. Adv., 2018, 4(1), eaao6657. 10.1126/sciadv.aao6657

[13] Zhu, J., Y. Tu, L. Cai, et al. Defect-assisted anchoring of Pt single atoms on MoS_2 nanosheets produces high-performance catalyst for industrial hydrogen evolution reaction, *Small*, 2021, **18**(4), 2104824. 10.1002/smll.202104824

[14] Anantharaj, S., K. Karthick, M. Venkatesh, et al. Enhancing electrocatalytic total water splitting at few layer Pt-NiFe layered double hydroxide interfaces, *Nano Energy*, 2017, **39**, 30-43. 10.1016/j.nanoen.2017.06.027

[15] Cheng, Q., C. Hu, G. Wang, et al. Carbon-defect-driven electroless deposition of Pt atomic clusters for highly efficient hydrogen evolution, *J. Am. Chem. Soc.*, 2020, **142**(12), 5594-5601. 10.1021/jacs.9b11524

[16] Tian, Y., Y. Luo, T. Wu, et al. Coupling interaction between precisely located Pt single-atoms/clusters and NiCo-layered double oxide to boost hydrogen evolution reaction, *Adv. Funct. Mater.*, 2024, 34, 2405919. 10.1002/adfm.202405919

[17] Zhong, W., B. Xiao, Z. Lin, et al. $RhSe_2$: a superior 3D electrocatalyst with multiple active facets for hydrogen evolution reaction in both acid and alkaline solutions, *Adv. Mater.*, 2021, **33**(9), 2007894. 10.1002/adma.202007894

[18] Tram Anh Duong, N., H. Tuan Nguyen, D. Thanh Tran, et al. Surface active sites and interphase engineering into metal oxide hydrates enabled by ions substitution for efficient water splitting, *Chem. Eng. J.*, 2024, **498**, 155287. 10.1016/j.cej.2024.155287

[19] Park, S., Y.-L. Lee, Y. Yoon, et al. Reducing the high hydrogen binding strength of

vanadium carbide MXene with atomic Pt confinement for high activity toward HER, *Appl. Catal. B-Environ. energy*, 2022, **304**, 120989. 10.1016/j.apcatb.2021.120989